Journal of Analytical and Applied Pyrolysis 175 (2023) 106207

Contents lists available at ScienceDirect

Journal of Analytical and Applied Pyrolysis

journal homepage: www.elsevier.com/locate/jaap

Rice husk-derived sodium hydroxide activated hierarchical porous biochar as an efficient electrode material for supercapacitors

Schindra Kumar Ray [a,*], Bishweshwar Pant [b,c], Mira Park [b,c], Bishnu Parsad Bastakoti [a,*]

[a] Department of Chemistry, North Carolina A & T State University, 1601 E Market St, Greensboro, NC 27411, USA
[b] Carbon Composite Energy Nanomaterials Research Center, Woosuk University, Wanju 55338, South Korea
[c] Woosuk Institute of Smart Convergence Life Care (WSCLC), Woosuk University, Wanju 55338, South Korea

ARTICLE INFO

Keywords:
Rice husk
Activated biochar
Pyrolysis
Porous carbon
Supercapacitor

ABSTRACT

In this study, one-step pyrolysis technique and NaOH chemical activation method were used to synthesize hierarchical porous biochar from rice husk. The existence of carbonaceous structure in biochar samples was confirmed by X-ray diffraction, field-emission scanning electron microscopy, elemental mapping, Raman spectroscopy, Brunauer-Emmett-Teller surface area, and X-ray photoelectron spectroscopy analysis. Activation of NaOH in rice husk biochar (ARB) sample suggested seven-fold enhancement of BET specific surface area (307.42 $m^2 g^{-1}$) as compared to rice husk biochar (RB). The NaOH activation also provides the enhancement of specific capacitance in RB. The boosting of supercapacitors (SCs) performance of ARB was proved by a larger loop in cyclic voltammetry and triangular shape along with a longer discharge time in galvanostatic charge-discharge curves as compared to RB. The electrode revealed excellent cyclic stability up to 4000 cycles with 94% retention. Furthermore, electrochemical impedance spectroscopy and galvanostatic charge-discharge curves showed evidence of electrode stability. The mechanisms related NaOH activation and enhancement of supercapacitor performance were well explained. These results suggest that NaOH treated RB could be promising low-cost electrode material for SCs application.

1. Introduction

Nowadays, supercapacitors (SCs) have attracted significant attention for the storage of clean and renewable energy to meet the global energy demands due to their excellent power density, fast charge/discharge rate, long cycle-life, reversibility, and high coulombic efficiency [1–5]. In this regard, electric double layer capacitance properties of porous carbon-based materials are promising SCs electrodes due to their excellent physicochemical stability, high surface area, good electrical conductivity, natural abundancy, and low cost [3,6]. The biomass-derived carbon materials (rice husk, tea leaves, Madhuca longifolia leaves, Solanum lycopersicum leaves, bamboo, saw dust, corncob, wastepaper, and flower etc.) are perfect options for SCs electrode because of several advantages such as biodegradability, controllable surface area/pore size, renewability, eco-friendly, and non-toxic [1,3,5,7–10].

Rice husk is one of the more abundant sources of biomass carbon materials. About 150 million tons of rice husk are produced during rice processing which is over 96% of rice husks annually worldwide [11,12]. The transformation of rice husk into biochar as a SCs electrode via pyrolysis technique helps the reduction of environmental pollution and disposal issues [3,13]. Rice husk biochar is porous, powdery, and lightweight [14]. It contains abundant oxygenated functional groups (-OH, C═O, and COOH) that can enhance the specific capacitance by increasing the wettability of carbon electrode [3]. Furthermore, the specific capacitance of rice husk biochar can be improved by chemical activation. It enhances the porosity and specific surface area that may associate with improvement of charging-discharging process or SCs performance via electric double layer mechanism [1,15]. Recently, biochar has been activated by several activating agents (KOH, NaOH, H_3PO_4, HF, and $ZnCl_2$ etc.) for enhancing the performance of SCs [15–18]. Among these agents, KOH is commonly used for biochar activation [10,17]. However, NaOH activated rice husk biochar for SCs application is hardly reported in literature. NaOH provides intercalation of metallic sodium that causes the generation of micropores or high energy sites via separation of carbon layers during activation reaction for improving the SCs performance [19]. So, the fabrication of NaOH-activated porous carbon from rice husk is good option for

* Corresponding authors.
E-mail addresses: schindrakumarray@gmail.com (S.K. Ray), bpbastakoti@ncat.edu (B.P. Bastakoti).

https://doi.org/10.1016/j.jaap.2023.106207
Received 18 March 2023; Received in revised form 9 July 2023; Accepted 4 October 2023
Available online 5 October 2023

improving the SCs performance.

Herein, we reported the fabrication of rice husk biochar and NaOH activated biochar by pyrolysis technique. All the biochar samples were well characterized by X-ray diffraction (XRD), field-emission scanning electron microscopy (FESEM), elemental mapping, Raman spectroscopy, Brunauer-Emmett-Teller (BET) surface area analyzer, pore volume, and X-ray photoelectron spectroscopy (XPS) analysis. In addition, the electrochemical performance of biochar samples was investigated by cyclic voltammetry (CV), galvanostatic charge-discharge (GCD), electron impedance spectroscopy (EIS), and cyclic stability. The mechanism related enhancement of SCs performance of NaOH activated rice husk biochar was explained.

2. Materials and methods

2.1. Chemicals and reagents

Sodium hydroxide (NaOH) and potassium hydroxide (KOH) were purchased from Sigma-Aldrich (NaOH reagent grade: ≥98%, and KOH reagent grade: ≥85%). In addition, hydrochloric acid (HCl) was obtained from Sigma Aldrich (ACS reagent, 37%). Polyvinylidene fluoride (PVDF) was taken from Thermo Fisher scientific. All the chemicals were used in experiment without any further purification.

2.2. Synthesis of rice husk biochar and activated rice husk biochar

The activated rice husk biochar was synthesized by using two steps (Fig. 1). In the 1st step, rice husk biochar was synthesized by pyrolysis technique. In this process, the rice husk was collected from a local market and washed with deionized water (DI) to remove impurities. It was dried in the oven at 105 °C for 24 h. Then, it was pulverized. 5 g of pulverized rice husk was put into an alumina boat and inserted into a tube furnace. The tube furnace was heated at 700° (10 °C/min, 0.5 L/min flow rate of carbon, 2 h carbonized, and anoxic condition). After that, it was cooled naturally and washed with 1 M HCl. After this treatment, it was dried in an oven (80 °C/12 h) and stored at room temperature. After a few hours, it was filtered (less than 100 mesh carbon) and washed with DI water to eliminate acid impurities. Finally, it was dried and grounded. This carbonized material was named as RB.

In the 2nd step, NaOH activation of rice husk biochar was performed. During NaOH activation, RB was mixed with NaOH with a mass ratio of 4:1. Then, the mixture was placed in an alumina boat and activated for 2 h N_2 flow at 700 °C. After cooling slowly to environmental temperature and washed with 1 M HCl. Furthermore, it was washed with water to remove excessive NaOH. It was dried in an oven at 105 °C for 24 h. The sample was named as ARB.

2.3. Material characterization

The X-ray diffraction (XRD) patterns of the samples were investigated using a powder X-ray diffractometer (Rigaku, Miniflex 600). The surface microstructure of as-prepared samples was determined using field-emission scanning electron microscopy (FESEM, JEOL, JSM-IT800). X-ray photoelectron spectroscopy (XPS) of the samples was carried out by Sigma Probe (Thermo scientific, Al K-alpha, and 200 eV). The specific Brunauer-Emmett-Teller (BET) surface areas and pore volume of the samples were recorded on a Micromeritics (TriStar II 3020). Raman spectrometer (DXR2xi, Thermo scientific, USA) was used to measure Raman spectra of the samples. The pyrolysis process was carried out on OTF-1200X (MTI CORPORATION). The electrochemical measurements were carried out on electrochemical analyzer (Versa STAT 4).

2.4. Electrochemical tests

For the preparation of biochar electrode, a piece of nickel foam was washed with 2 M HCl, water, and ethanol to remove the impurities. The working electrode (4 mg) was fabricated by mixing as-synthesized biochar samples, acetylene black, and polyvinylidene fluoride (PVDF) along with the mass ratio 80:10:10 in N-methyl-2-pyrrolidone (NMP). After that, the slurry was deposited on nickel foam using a micropipette and dried in an oven at 60 °C for 12 h. The electrochemical measurements (CV, GCD, EIS, and stability) were investigated by using a three-electrode system at room temperature in a 6 M KOH solution using Versastat3. The biochar loaded nickel foam (1 ×1) was used as a working electrode whereas Ag/AgCl and Pt wire were applied as reference and counter electrodes, respectively. The specific capacitance of the electrode material was calculated from GCD curves using the following equation [4,20,21].

$$Cs = \frac{I.\Delta t}{m.\Delta V}$$

where '*Cs*', '*I*', 'Δt', 'm', and ΔV represent the specific capacitance (F/g), charge/discharge current (A), discharge time (s), mass of the

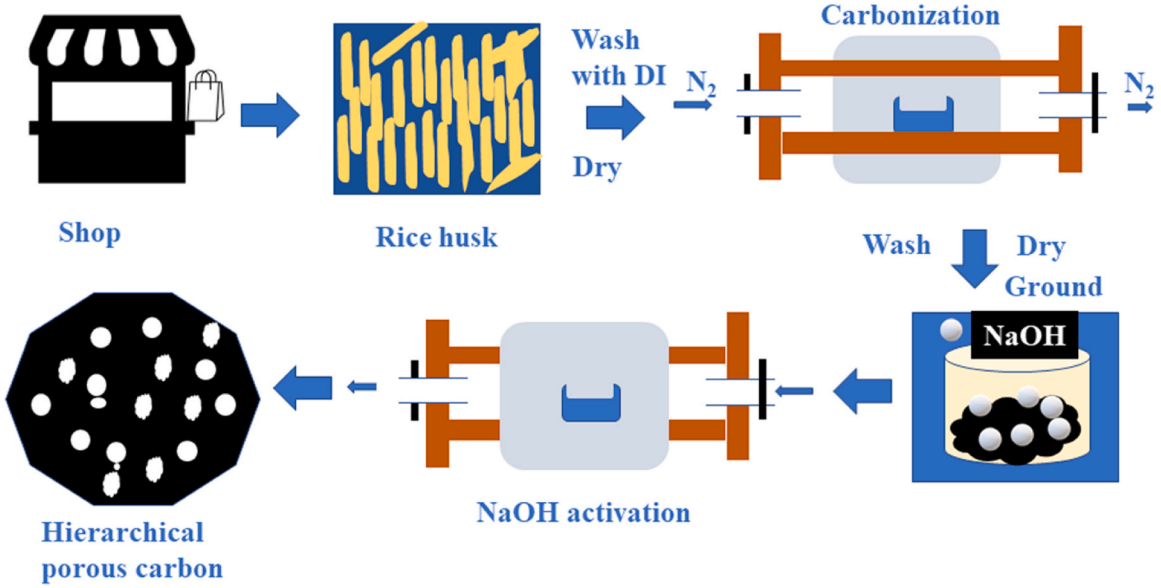

Fig. 1. A sketch of the synthesis procedure for NaOH activated rice husk biochar.

material (g), and potential window (V), respectively.

3. Results and discussion

Fig. 2a. shows the XRD patterns of the as-prepared RB and ARB samples. The XRD peak at $2\theta = 20^\circ - 30^\circ$ indicates (002) graphite plane that suggests the stacking structure of the aromatic layer in samples. In addition, the graphite crystallite plane (100) at $2\theta = 43.31^\circ$ reveals the decomposition of cellulose in the raw material at high pyrolysis temperature into carbon structure. [22,23]. The remaining peaks in samples may indicate the presence of miscellaneous inorganic compounds. Also, the XRD peaks show the presence of heterogenous surface. These results indicate no change in XRD patterns even after the activation of RB by NaOH. Moreover, micro-graphitic structures in biochar samples facilitate electron transfer which is beneficial for SCs performance [24].

According to Fig. 2b, the Raman spectra of samples demonstrate the two intense peaks, D and G bands [25,26]. The D band at 1357.79 cm^{-1} indicates the defects in graphite structures in samples. It also informs the existence of aromatic systems with linked aromatic rings which is equivalent to graphite sheet [27]. The G band at 1582.12 cm^{-1} suggests the vibrations of pure graphite. These results give the evidence of carbonaceous structure in the samples [28]. The N_2 adsorption/desorption graphs appeared tailing that demonstrates the significant increase in adsorption capacity (Fig. 3a) with type H4 hysteresis loop. It may associate with capillary condensation of mesopores/micropores in the samples [29,30]. The BET specific surface area of RB and ARB was 44.82 and 307.42 $m^2\ g^{-1}$. The specific surface area of ARB was about 7 times higher than the RB. Also, Fig. 3b suggested the presence of porous structure in biochar samples. The development of a narrow pore range in the NaOH-activated RB sample was observed. The use of NaOH as the activator significantly increases the specific surface area and porosity that is beneficial for electrochemical charge storage.

The mechanism-related porosity can be observed by the etching reaction between the carbon atoms and melted NaOH. During the activation process, molten NaOH is first contacted with the carbon precursor. NaOH may be transformed into Na_2O and H_2O by dehydration reaction with the increase in temperature. In addition, redox reactions can occur between NaOH and biochar to form Na_2CO_3, Na_2O, and H_2. Also, carbon atoms may interact with NaOH to produce CO and H_2. Na_2CO_3 decomposes into Na_2O and H_2O. Furthermore, carbon atoms could react with Na_2O and Na_2CO_3 to form CO and Na. The metallic Na atom becomes vapor at a high temperature (700 °C) and intercalate/diffuse into the carbon lattice of biochar and the development of pore occurs [24,31].

The evidence of pore was also supported by the FESEM micrographs of RB and ARB samples (Fig. 4). The agglomerated heterogenous morphology, with particles ranging a few micrometers, was observed (Figs. 4a and 4c). According to Figs. 4b and 4d, the hierarchical porous structure of RB and ARB samples was clearly indicated by the presence of pores (~1 μm) with several open cavities (5–10 μm). In addition, a large number of pores were found in ARB than in RB. In ARB, a great number of 3D architectures as well as interconnected network-like structures were found as compared to RB. These results indicate that activation of RB provides the enhancement of macro- and microporosity, which is extremely useful for strong performance in energy storage applications [6].

The XPS spectra of the biochar samples were used to analyze the chemical composition and chemical state of the elements and the results were presented in Fig. 5. The C 1 s spectra of the samples can be divided into two peaks. The peaks, 284.79 eV (RB) and 284.72 eV (ARB) represent the C═C/C-C of graphitic or amorphous carbon. In addition, the presence of sp2 carbon (C═O) was observed in RB and ARB samples at 285.48 eV and 285.39 eV, respectively (Figs. 5a and 5c) [32]. The O 1 s peak could be deconvoluted into two different peaks, assigning to C═O (RB: 532.79 eV and ARB: 532.46 eV) and C-O ether like bond in hydroxyl group (RB: 534.08 eV and ARB: 534.02 eV) (Figs. 5b and 5d) [33]. Furthermore, the survey spectra indicates the presence of carbon and oxygen in samples (Fig. 5e).

The electrochemical performance of the as-synthesized biochar samples was analyzed using CV, GCD, and EIS measurements, based on a three-electrode system. Fig. 6a shows the CV curves of the as-synthesized RB and ARB samples in 6 M KOH solution at a scan rate of 10 mV/s. The CV curves of electrodes reveal a rectangular-like shape without a hump, suggesting a typical electrical double-layer capacitive nature. In addition, the ARB electrode demonstrates a larger area under the CV curve than that of RB electrode providing evidence of higher specific capacitance [34]. The CV of ARB electrode at different scan rates (10 mV/s- 100 mV/s) in a potential window of 0.0 V to − 1.0 V is given in Fig. 6b. As seen in Fig. 6b, the ARB electrode presented a rectangular shape, even at a high scan rate of 100 mV/s, suggesting a good rate characteristic. It suggests the highly graphitized structure with several pores in the sample that can facilitate the fast ion transport for enhancement of SCs performance [31]. This CV results showed the excellent rate capability of the ARB electrode. The possible reasons may be associated with enhancement of adsorption and desorption process with increase in porosity and surface area [5].

Galvanostatic charge-discharge (GCD) curves were measured to further investigate the electrochemical behavior of the as-prepared samples (Figs. 6c and 6d). The comparison of GCD graphs for RB and ARB electrodes is presented in Fig. 6c. The nature of the GCD curve was well matched with CV curves. In both cases, the GCD curves showed a triangular curve, suggesting a double-layer capacitor. The longer discharge time in the case of ARB than that of RB indicates a higher capacitance. GCD curves of ARB electrode at different current densities (0.25, 0.5, 1, 2, 3, 4, 5, 8, and 10 A/g) are given in Fig. 6d. These curves showed the symmetric triangular shape without obvious IR drops as an

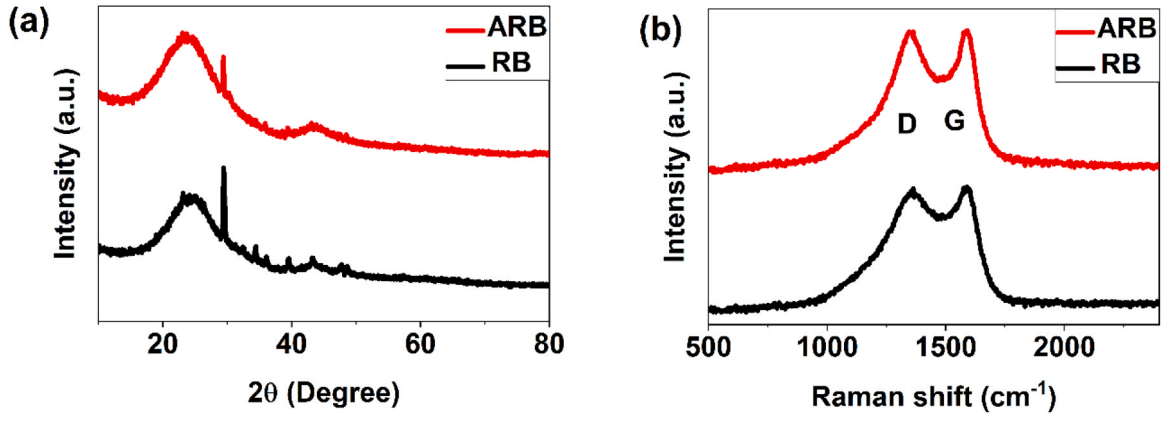

Fig. 2. (a) XRD patterns and (b) Raman spectra of samples.

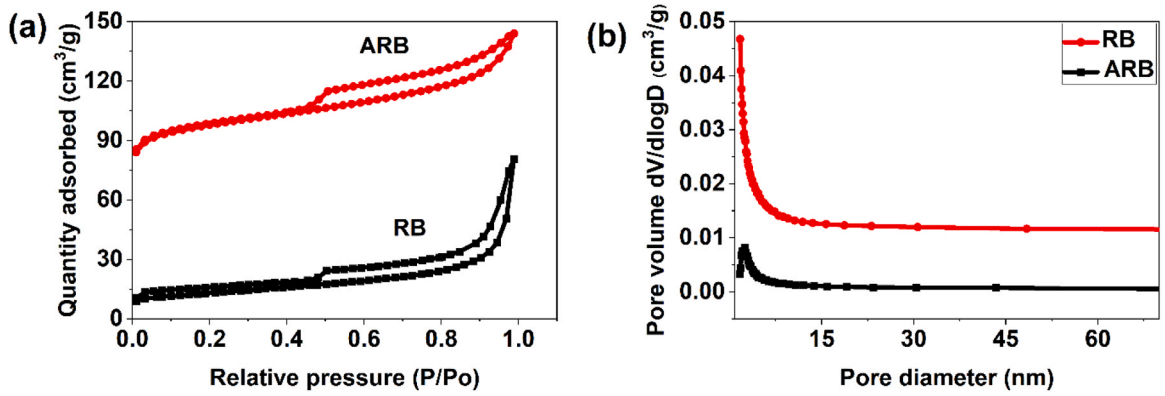

Fig. 3. (a) N_2 adsorption-desorption isotherms and (b) pore size distribution of biochar samples. of samples.

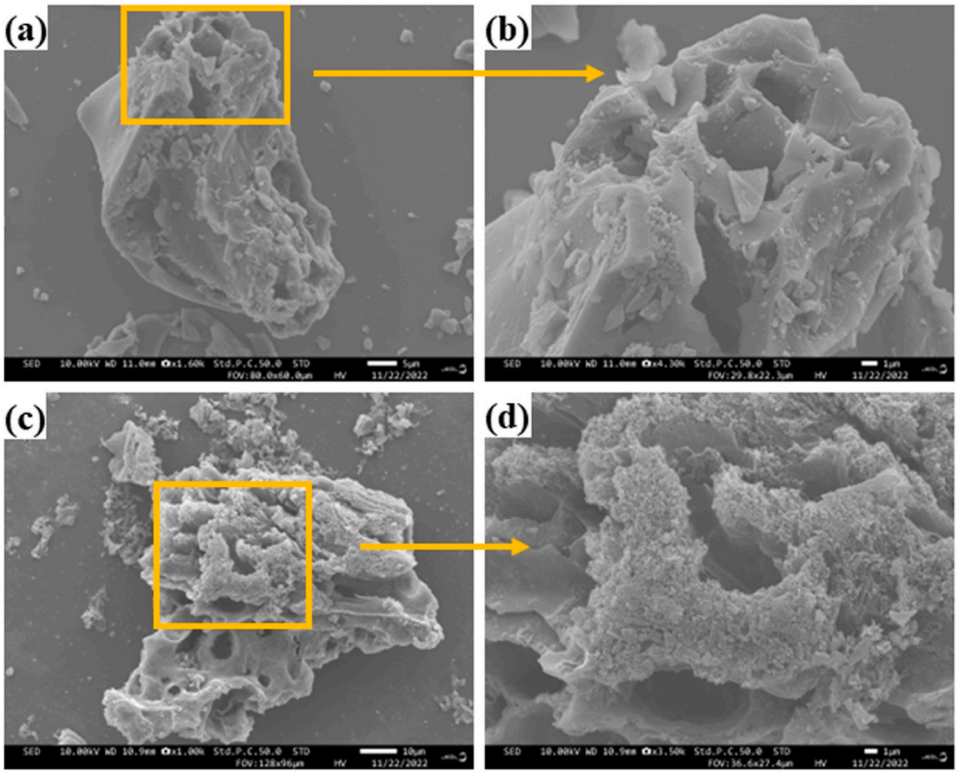

Fig. 4. FESEM images of samples. (a) RB, (b) magnified part of RB, (c) ARB, and (d) maginified of ARB.

evidence of the supercapacitive properties of porous carbons. It also suggests the great capacitive reversibility with excellent charge-discharge efficiency of the sample [6,34].

The specific capacitance graph of RB and ARB electrodes was presented in Fig. 7a. The specific capacitance of RB electrode was 60, 53, 45, 30, 21, 12, and 10 F/g at 0.25, 0.5, 1, 2, 3, 4, and 5 A/g current densities, respectively. Furthermore, the specific capacitance of ARB electrode revealed 112, 104, 95, 86, 76, 65, 58, 43, 36, and 30 F/g at 0.25, 0.5, 1, 2, 3, 4, 5, 8, 10, and 12 A/g current densities, respectively. These results demonstrate the improvement of specific capacitance of rice husk biochar by NaOH activation. The improved electrochemical properties in the case of ARB are mainly attributed to its porous morphology. The highly graphitized structure with several pores in sample that can facilitate the fast ion transport for enhancement of SCs performance [5,31]. Compared to RB, the ARB possesses well-arranged 3D architecture along with interconnected network. This unique combination of microporous and mesoporous properties shortens the ion transportation path and allows easy and fast movement of ions, resulting in enhanced capacitance.

The retention capacities of RB and ARB electrodes are shown in Fig. 7b. The ARB and RB electrodes retained 94% and 91% of their initial capacitance, respectively after 4000 cycles, suggesting excellent cyclic stability. The slight decrease in specific capacitance after 4000 cycles is attributed to the swelling of pore network, gradual penetration of electrolyte ions into active sites of electrode materials, and continuous interaction of pores with the electrolyte during charging-discharging cycles [1]. To further confirm the stability of the electrode material, we compared the EIS and GCD of the ARB electrodes before and after the stability test. Fig. 7c shows the EIS spectrum of ARB before and after stability tests. ARB electrode showed a slightly larger arc radius at the high frequency region after stability test, suggesting a slight reduction in the conductivity of the material. Also, there is no significant change in electron transfer process after 4000 cycles. The GCD curve given in Fig. 7d also verifies the results obtained from the stability test. This

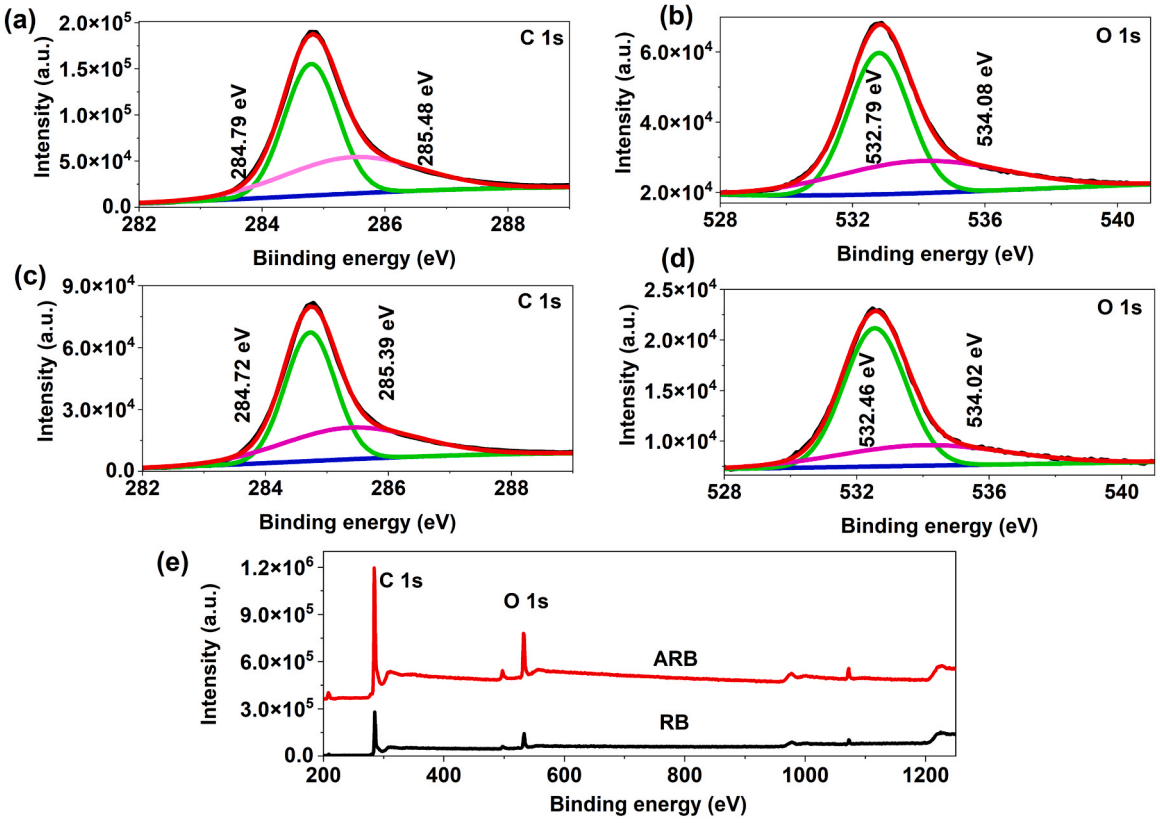

Fig. 5. XPS of RB (a: C 1 s and b: O 1 s), ARB (c: C 1 s and d: O 1 s) and survey spectra (e) of samples.

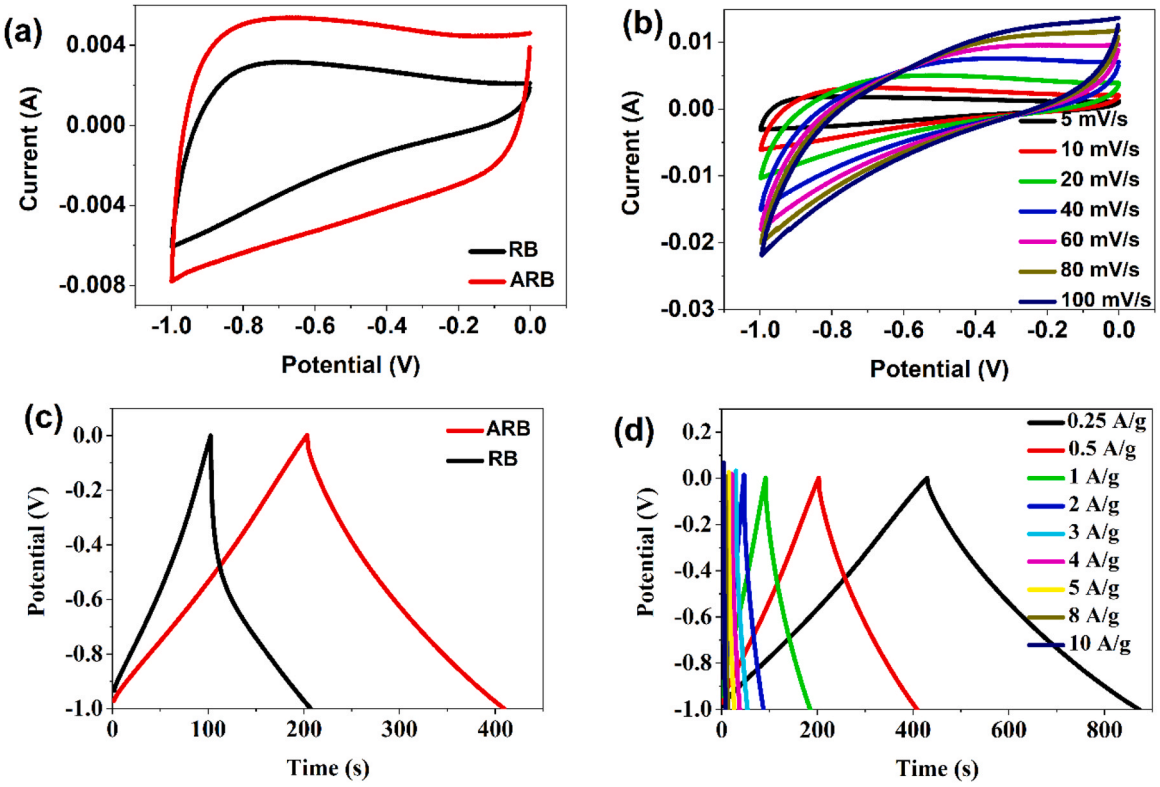

Fig. 6. (a) CV curves of RB and ARB at 10 mV/s, (b) CV curves of ARB electrode at different scan rates, (c) GCD curves of RB and ARB at 0.5 A/g, (d) GCD curves of ARB electrode at different current densities.

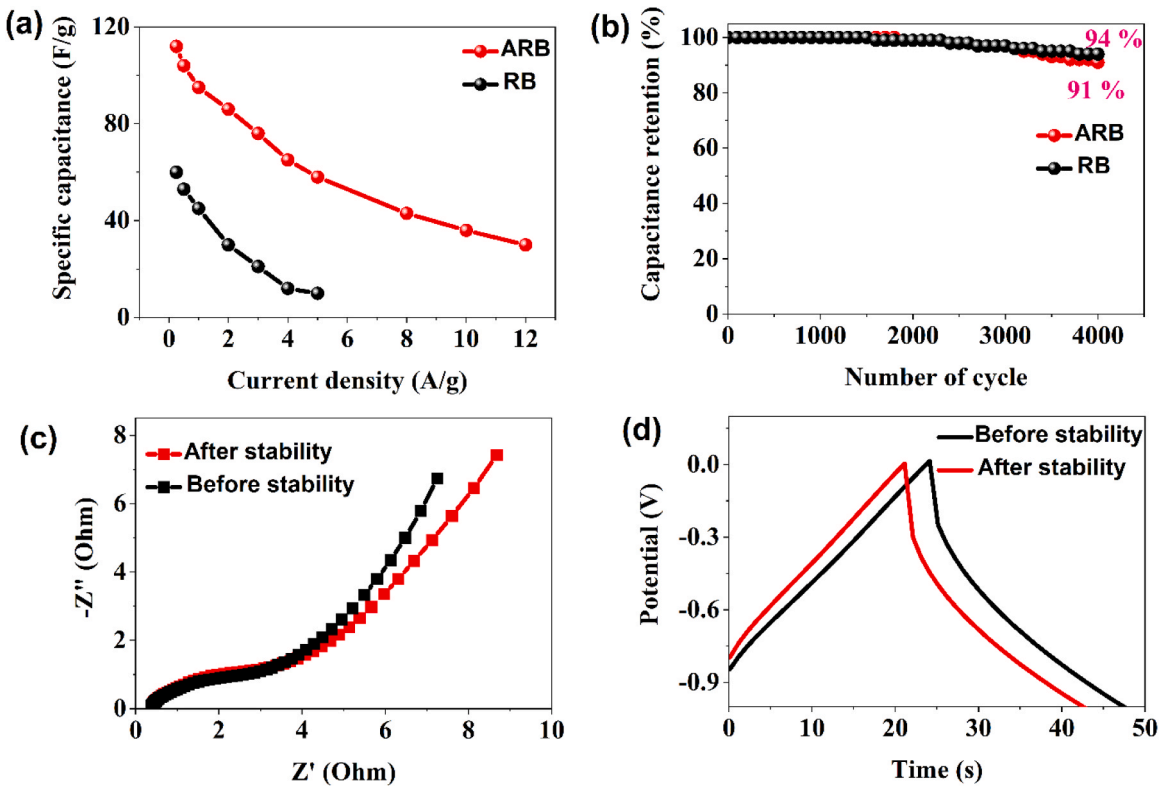

Fig. 7. (a) Specific capacitance of RB and ARB at different current densities, (b) GCD curves ARB and RB, (c) EIS curve of ARB before and after stability, and (d) GCD curves of ARB before and after stability.

remarkable cyclic stability demonstrated that NaOH activated rice husk biochar could be considered as a low-cost electrode material for SCs. Furthermore, our results were compared with other published research works related with NaOH/KOH activated rice husk biochar in Table 1. According this table, our ARB presented superior porous structure, great stability, and good specific capacitance as compared to other published litertaures. The superior features suggest that ARB is a promising electrode material for supercapacitor.

Table 1
Comparison of specific capacitance of alkali activated rice husk biochar.

Activating agent	Synthesis /activation method	Electrolyte	Specific capacitance	Stability	Ref.
KOH	Carbonization: 550 °C /4 h and activation: 800 °C /1 h	KOH (6 M)	250 F/g at 1 A/g	80% after 10,000 cycles	[35]
KOH	Carbonization: 400 °C /3 h and activation: 800 °C/0.5 h	KOH (6 M)	224 F/g at 0.5 A/g	86%/ after 10,000 cycles	[36]
KOH	Carbonization: 600 °C/2 h	H2SO4 (0.1 M)	113.5 F/g	95% after 1000 cycles	[37]
KOH	Carbonization: 500 °C /5° min^{-1}	SPVA-HRG	80.2 F/g at 0.05 A/g	-	[38]
NaOH	Carbonization: 600 °C /1 h and activation: 750 °C /1 h	KOH (6 M)	51.4 F/g at 0.5 A/g	99.6% after 20,000 cycles	[39]
NaOH	Carbonization: 800 °C /2 h and activation: 100 °C /2 h	KOH (6 M)	86 F/g at 1 A/g	78% after 5000 cycles	[40]
NaOH	Carbonization: 700 °C /2 h and activation: 700 °C/2 h	KOH (6 M)	112 F/g at 0.5 A/g	94% after 4000 cycles	Our work

4. Conclusions

In summary, NaOH-activated biochar sample was synthesized by the pyrolysis technique. The biochar materials were well characterized by XRD, FESEM, elemental mapping, Raman, BET, and XPS. The electrochemical properties of samples were analyzed by CV, EIS, GCD, and cyclic stability measurements. The results clearly reveal the enhancement of surface area and porosity by activating RB by NaOH that can boost the specific capacitance, rate capability, and long-term stability with superior retention capability. This study provides a simple and efficient strategy to synthesize the NaOH-activated rice husk biochar from rice husk waste for excellent and stable supercapacitor performance that may develop a low-cost energy storage device in the future.

CRediT authorship contribution statement

Schindra Kumar Ray: Conceptualization, Methodology, Validation, Formal analysis, Investigation, Resources, Data curation, Writing – original draft, Writing – review & editing. **Bishweshwar Pant**: Funding acquisition, Electrochemical measurements, Writing – review & editing. **Mira Park:** Funding acquisition, Electrochemical measurements, Writing – review & editing. **Bishnu Prasad Bastakoti:** Funding acquisition, Supervision, Writing – review & editing.

Declaration of Competing Interest

The authors declare that they have no known competing financial interests or personal relationships that could have appeared to influence the work reported in this paper.

Data Availability

The authors do not have permission to share data.

Acknowledgments

This research was supported by National Science Foundation Research Initiation Award (2000310) and the excellence in Research Award (2100710) USA. This work was also supported by the National Research Foundation of Korea (NRF) grant funded by the Korea government (MSIT) (NRF-2019R1A2C1004467).

References

[1] R.K.Dutta Atika, Oxygen-rich porous activated carbon from eucalyptus wood as an efficient supercapacitor electrode, Energy Technol. 9 (2021) 2100463, https://doi.org/10.1002/ente.202100463.
[2] J.R. Miller, P. Simon, Electrochemical capacitors for energy management, Science 80 (321) (2008) 651–652, https://doi.org/10.1126/science.1158736.
[3] W.J. Liu, H. Jiang, H.Q. Yu, Emerging applications of biochar-based materials for energy storage and conversion, Energy Environ. Sci. 12 (2019) 1751–1779, https://doi.org/10.1039/c9ee00206e.
[4] S.K. Ray, B. Pant, M. Park, J. Hur, S.W. Lee, Cavity-like hierarchical architecture of WS2/α-NiMoO4 electrodes for supercapacitor application, Ceram. Int. 46 (2020) 19022–19027, https://doi.org/10.1016/j.ceramint.2020.04.232.
[5] B. Pant, G.P. Ojha, J. Acharya, H.R. Pant, M. Park, Lokta paper-derived free-standing carbon as a binder-free electrode material for high-performance supercapacitors, Sustain. Mater. Technol. 33 (2022), e00450, https://doi.org/10.1016/j.susmat.2022.e00450.
[6] Y. Xiao, M. Zheng, X. Chen, H. Feng, H. Dong, H. Hu, Y. Liang, S.P. Jiang, Y. Liu, Hierarchical porous carbons derived from rice husk for supercapacitors with high activity and high capacitance retention capability, ChemistrySelect 2 (2017) 6438–6445, https://doi.org/10.1002/slct.201701275.
[7] S. Rawat, R.K. Mishra, T. Bhaskar, Biomass derived functional carbon materials for supercapacitor applications, Chemosphere 286 (2022), 131961, https://doi.org/10.1016/j.chemosphere.2021.131961.
[8] M.S. Priya, R. Rajalakshmi, Comparison of porous carbon electrodes derived from madhuca longifolia leaves by hydrothermal technique and direct pyrolysis techniques, Asian J. Chem. 35 (2023) 1037–1043, https://doi.org/10.14233/ajchem.2023.27597.
[9] P. Divya, R. Rajalakshmi, Renewable low cost green functional mesoporous electrodes from Solanum lycopersicum leaves for supercapacitors, J. Energy Storage 27 (2020), 101149, https://doi.org/10.1016/j.est.2019.101149.
[10] M. Shanmuga Priya, P. Divya, R. Rajalakshmi, A review status on characterization and electrochemical behaviour of biomass derived carbon materials for energy storage supercapacitors, Sustain. Chem. Pharm. 16 (2020), 100243, https://doi.org/10.1016/j.scp.2020.100243.
[11] K. Herrera, L.F. Morales, N.A. Tarazona, R. Aguado, J.F. Saldarriaga, Use of biochar from rice husk pyrolysis: part a: recovery as an adsorbent in the removal of emerging compounds, ACS Omega 7 (2022) 7625–7637, https://doi.org/10.1021/acsomega.1c06147.
[12] R. Chen, S.S.C. Congress, G. Cai, W. Duan, S. Liu, Sustainable utilization of biomass waste-rice husk ash as a new solidified material of soil in geotechnical engineering: a review, Constr. Build. Mater. 292 (2021), 123219, https://doi.org/10.1016/j.conbuildmat.2021.123219.
[13] E. Menya, P.W. Olupot, H. Storz, M. Lubwama, Y. Kiros, Production and performance of activated carbon from rice husks for removal of natural organic matter from water: a review, Chem. Eng. Res. Des. 129 (2018) 271–296, https://doi.org/10.1016/j.cherd.2017.11.008.
[14] A.G. Gebretatios, A.R. Kadiri Kanakka Pillantakath, T. Witoon, J.W. Lim, F. Banat, C.K. Cheng, Rice husk waste into various template-engineered mesoporous silica materials for different applications: a comprehensive review on recent developments, Chemosphere 310 (2023), 136843, https://doi.org/10.1016/j.chemosphere.2022.136843.
[15] R. Mehdi, A.H. Khoja, S.R. Naqvi, N. Gao, N.A.S. Amin, A review on production and surface modifications of biochar materials via biomass pyrolysis process for supercapacitor applications, Catalysts 12 (2022) 798, https://doi.org/10.3390/catal12070798.
[16] E. Scapin, G.P. da, S. Maciel, A.D.S. Polidoro, E. Lazzari, E.V. Benvenutti, T. Falcade, R.A. Jacques, Activated carbon from rice husk biochar with high surface area, Biointerface Res. Appl. Chem. 11 (2021) 10265–10277, https://doi.org/10.33263/BRIAC113.1026510277.
[17] X. Li, J. Zhang, B. Liu, Z. Su, A critical review on the application and recent developments of post-modified biochar in supercapacitors, J. Clean. Prod. 310 (2021), 127428, https://doi.org/10.1016/j.jclepro.2021.127428.
[18] L. Haghighi Poudeh, I. Berktas, H.Q. Ali, B. Saner Okan, M. Yıldız, Toward next-generation carbon-based materials derived from waste and biomass for high-performance energy applications, Energy Technol. 8 (2020), https://doi.org/10.1002/ente.202000714.
[19] K. Takeuchi, M. Fujishige, N. Ishida, Y. Kunieda, Y. Kato, Y. Tanaka, T. Ochi, H. Shirotori, Y. Uzuhashi, S. Ito, K. ichi Oshida, M. Endo, High porous bio-nanocarbons prepared by carbonization and NaOH activation of polysaccharides for electrode material of EDLC, J. Phys. Chem. Solids 118 (2018) 137–143, https://doi.org/10.1016/j.jpcs.2018.02.050.
[20] B. Pant, G.P. Ojha, J. Acharya, M. Park, Eggshell membrane templated synthesis of Ni/MoC decorated carbon fibers with good electrochemical behavior, Int. J. Hydrog. Energy 46 (2021) 2774–2782, https://doi.org/10.1016/j.ijhydene.2020.10.139.
[21] B. Pant, G.P. Ojha, J. Acharya, M. Park, Preparation, characterization, and electrochemical performances of activated carbon derived from the flower of Bauhinia variegata L for supercapacitor applications, Diam. Relat. Mater. 136 (2023), 110040, https://doi.org/10.1016/j.diamond.2023.110040.
[22] S. Zhang, J. Wang, Removal of chlortetracycline from water by immobilized Bacillus subtilis on honeysuckle residue–derived biochar, Water Air Soil Pollut. 232 (2021) 1–14, https://doi.org/10.1007/s11270-021-05193-1.
[23] G. Ravenni, Z. Sárossy, S. Sanna, J. Ahrenfeldt, U.B. Henriksen, Residual gasification char applied to tar reforming in a pilot-scale gasifier: performance and evolution of char properties for perspective cascade uses, Fuel Process. Technol. 210 (2020), 106546, https://doi.org/10.1016/j.fuproc.2020.106546.
[24] C. Quan, R. Su, N. Gao, Preparation of activated biomass carbon from pine sawdust for supercapacitor and CO_2 capture, Int. J. Energy Res. 44 (2020) 4335–4351, https://doi.org/10.1002/er.5206.
[25] Q.Q. Li, X. Zhang, W.P. Han, Y. Lu, W. Shi, J.B. Wu, P.H. Tan, Raman spectroscopy at the edges of multilayer graphene, Carbon N. Y 85 (2015) 221–224, https://doi.org/10.1016/j.carbon.2014.12.096.
[26] K.B. Rai, I.B. Khadka, A.R. Koirala, S.K. Ray, Insight of cleaning, doping and defective effects on the graphene surface by using methanol, Adv. Mater. Res. 10 (2021) 283–292, https://doi.org/10.12989/amr.2021.10.4.283.
[27] X. Li, J. ichiro Hayashi, C.Z. Li, FT-Raman spectroscopic study of the evolution of char structure during the pyrolysis of a victorian brown coal, Fuel 85 (2006) 1700–1707, https://doi.org/10.1016/j.fuel.2006.03.008.
[28] A.C. Ferrari, Raman spectroscopy of graphene and graphite: disorder, electron-phonon coupling, doping and nonadiabatic effects, Solid State Commun. 143 (2007) 47–57, https://doi.org/10.1016/j.ssc.2007.03.052.
[29] Z. Husain, A.R. Shakeelur Raheman, K.B. Ansari, A.B. Pandit, M.S. Khan, M. A. Qyyum, S.S. Lam, Nano-sized mesoporous biochar derived from biomass pyrolysis as electrochemical energy storage supercapacitor, Mater. Sci. Energy Technol. 5 (2022) 99–109, https://doi.org/10.1016/j.mset.2021.12.003.
[30] L. Zhu, N. Zhao, L. Tong, Y. Lv, Structural and adsorption characteristics of potassium carbonate activated biochar, RSC Adv. 8 (2018) 21012–21019, https://doi.org/10.1039/c8ra03335h.
[31] Y. Cao, K. Wang, X. Wang, Z. Gu, Q. Fan, W. Gibbons, J.D. Hoefelmeyer, P. R. Kharel, M. Shrestha, Hierarchical porous activated carbon for supercapacitor derived from corn stalk core by potassium hydroxide activation, Electrochim. Acta 212 (2016) 839–847, https://doi.org/10.1016/j.electacta.2016.07.069.
[32] N.S. Kumar, H.M. Shaikh, M. Asif, E.H. Al-Ghurabi, Engineered biochar from wood apple shell waste for high-efficient removal of toxic phenolic compounds in wastewater, Sci. Rep. 11 (2021) 1–18, https://doi.org/10.1038/s41598-021-82277-2.
[33] H. Wang, H. Wang, H. Zhao, Q. Yan, Adsorption and Fenton-like removal of chelated nickel from Zn-Ni alloy electroplating wastewater using activated biochar composite derived from Taihu blue algae, Chem. Eng. J. 379 (2020), 122372, https://doi.org/10.1016/j.cej.2019.122372.
[34] F. Yao, D.T. Pham, Y.H. Lee, Carbon-based materials for lithium-ion batteries, electrochemical capacitors, and their hybrid devices, ChemSusChem 8 (2015) 2284–2311, https://doi.org/10.1002/cssc.201403490.
[35] H. Xu, B. Gao, H. Cao, X. Chen, L. Yu, K. Wu, L. Sun, X. Peng, J. Fu, Nanoporous activated carbon derived from rice husk for high performance supercapacitor, J. Nanomater. 2014 (2014) 1–8, https://doi.org/10.1155/2014/714010.
[36] J. Chen, J. Liu, D. Wu, X. Bai, Y. Lin, T. Wu, C. Zhang, D. Chen, H. Li, Improving the supercapacitor performance of activated carbon materials derived from pretreated rice husk, J. Energy Storage 44 (2021), 103432, https://doi.org/10.1016/j.est.2021.103432.
[37] N.A.M. Barakat, O.M. Irfan, H.M. Moustafa, H3PO4/KOH activation agent for high performance rice husk activated carbon electrode in acidic media supercapacitors, Molecules 28 (2022) 296, https://doi.org/10.3390/molecules28010296.
[38] V.K. Nersu, B.R. Annepu, S.S.B. Patcha, S.S. Rajaputra, Rice husk char as a potential electrode material for supercapacitors, J. Electrochem. Sci. Eng. 12 (2022) 451–462, https://doi.org/10.5599/jese.1310.
[39] Z. Chen, X. Wang, B. Xue, W. Li, Z. Ding, X. Yang, J. Qiu, Z. Wang, Rice husk-based hierarchical porous carbon for high performance supercapacitors: The structure-performance relationship, Carbon N. Y 161 (2020) 432–444, https://doi.org/10.1016/j.carbon.2020.01.088.
[40] W. Zhang, N. Lin, D. Liu, J. Xu, J. Sha, J. Yin, X. Tan, H. Yang, H. Lu, H. Lin, Direct carbonization of rice husk to prepare porous carbon for supercapacitor applications, Energy 128 (2017) 618–625, https://doi.org/10.1016/j.energy.2017.04.065.